DOI: 10.1021/cg900869f

CRYSTAL GROWTH & DESIGN Article

2010, Vol. 10 237–243

# Field Emission and Electrical Switching Properties of Large-Area CuTCNQ Nanotube Arrays

Huibiao Liu,*,† Zheng Liu,§ Xuemin Qian,†,‡ Yanbing Guo,† Shuang Cui,† Lianfeng Sun,§ Yinglin Song,‡ Yuliang Li,*,† and Daoben Zhu†

†*CAS Key Laboratory of Organic Solid, Beijing National Laboratory for Molecular Sciences (BNLMS), Institute of Chemistry, Chinese Academy of Sciences, Beijing 1000190, P. R. China,* §*National Center for Nanoscience and Technology, Chinese Academy of Sciences, Beijing 100190, P. R. China, and* ‡*School of Physical Science and Technology, Suzhou University, Suzhou, Jiangsu Province, 215006, P. R. China*

*Received July 24, 2009; Revised Manuscript Received September 20, 2009*

**ABSTRACT:** Large-area single crystalline CuTCNQ nanotube arrays (ca. 24 $cm^2$) have been fabricated using an in situ organic vapor solid phase reaction by instantaneous heating (TCNQ = 7,7,8,8-tetracyanoquinodimethane). The size of CuTCNQ nanotubes can tuned by controlling the reaction temperature. The facile approach provides an important finding for large-area synthesis of vertically aligned array organic nanotubes on conductive substrate, which is crucial to the direct fabricating of electronic and optoelectronic devices for a wide variety of potential applications. The CuTCNQ nanotube arrays exhibited excellent field emission (FE) properties and size-dependent FE properties were observed. The devices based on these highly ordered CuTCNQ nanotube arrays have been demonstrated and have exhibited excellent electrical switching effects. The maximal ON/OFF ratio of CuTCNQ nanotube arrays is about 1100. The morphology-dependent electrical-switching properties of the CuTCNQ nanotube arrays were investigated. These results suggest that the CuTCNQ nanotube array can be expected to find promising applications as field emitters and nanoelectronic devices.

## Introduction

Among organic one-dimensional architectures, increasing interest has been focused on organic nanotubes due to their higher surface area and hollow structure.[1,2] In particular, large area, vertically aligned nanotube arrays on a conductive substrate are expected to have high performance in solar cells, field emitters, field-effect transistor, and luminescent diodes because of their well-defined channels for carriers.[2] However, only a few examples are able to form very small-area organic nanotube arrays by employing the typical self-assembly and template-based methods as reported previously.[3] Those organic nanotubes prepared by above-mentioned methods are always free-standing, and very difficult to be directly used in nanodevices because they cannot orderly locate on the solid surface after the removal of the templates. Therefore, it still requires further effort to explore a facile and versatile synthetic method to obtain aligned organic nanotube arrays.

Among the organic materials, the organic charge transfer complex CuTCNQ (TCNQ = 7,7,8,8-tetracyanoquinodimethane) has unique electrical and optical properties and has been applied as optical and electrical recording media, which has led to renewed interest.[4] Various methods such as vacuum vapor deposition, spontaneous electrolysis techniques, and electrochemistry have been employed to yield a host of different CuTCNQ morphologies such as nanowires, nanorods, and nanoneedles.[4e−q] However, there have been no studies on the preparation of large-area of CuTCNQ nanotube arrays on conductive substrates. Recent work from this laboratory has focused on organic vapor solid phase reactions for the controlled synthesis of CuTCNQ nanostructures and has found their excellent field emission (FE) properties.[4f,i,p,q] In this work, we conducted in situ organic solid-reaction-initiated unidirectional growth of aligned CuTCNQ nanotubes on copper foil under instantaneous heating conditions leading to form large-area free-standing nanotube arrays (ca. 24 $cm^2$). Meanwhile, we also achieved control of the length and size of CuTCNQ nanotube arrays. This new method ensures that the nanotubes in the arrays are in direct contact with the conductive substrate and provide a continuous pathway for carrier transport. The combined properties enable the nanotube to have very specific applications on direct construction devices on large-area arrays. We demonstrate that these vertically aligned CuTCNQ nanotube arrays indeed exhibit excellent FE properties and size-dependent FE properties were observed. The devices based on these CuTCNQ nanotube arrays have exhibited morphology-dependent electrical-switching properties. The maximum ON/OFF ratio of CuTCNQ nanotube arrays is up to 1100. Therefore, large-area CuTCNQ nanotube arrays may be expected to be suitable for electronic and optoelectronic devices such as field emitters, high density information storage, and nanoscale switching devices.

## Experimental Section

**Chemicals.** TCNQ was obtained from Aldrich. Copper foil was obtained from Beijing Chemicals Corp. and used with ultrasonicated in 0.1 M HCl, pure water, acetone, and ethanol, respectively. All solvents in this study were purchased from Beijing Chemicals Corp. and used without further purification.

**Measurements.** Scanning electron microscopic (SEM) measurements were performed using a Hitachi S4300 field emission scanning electron microscope (FE-SEM). Transmission electron microscopic (TEM) measurements and selected-area electron diffraction (SAED) patterns were performed using a JEOL JEM-1011. For TEM studies, pieces of samples A−C were ultrasonicated in 2 mL of

*To whom correspondence should be addressed. E-mail: liuhb@iccas.ac.cn, (H.L.)ylli@iccas.ac.cn (Y.L.).



Published on Web 10/13/2009

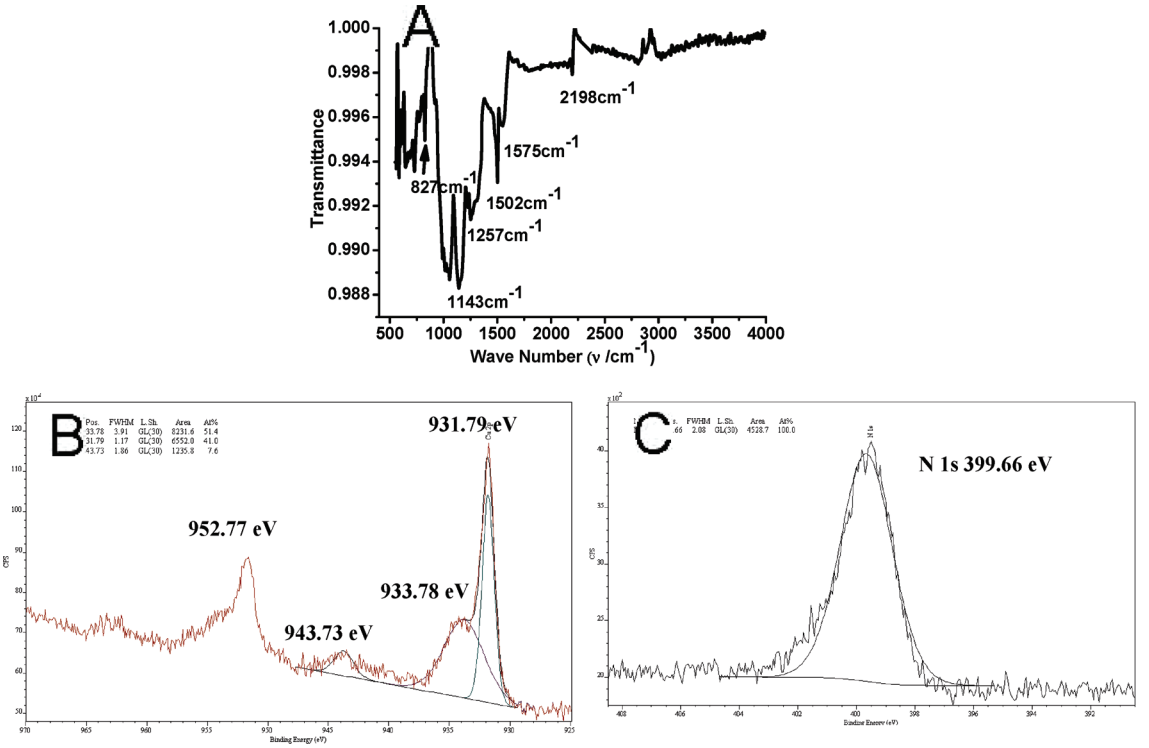


**Figure 1.** (A) FT-IR spectra. XPS data in the Cu $2p_{3/2}$ and $2p_{1/2}$ (A) and $N_{1s}$ (B) for CuTCNQ nanotube arrays (Sample A).

ethanol, respectively, a drop of ethanol solution of samples was dripped on a carbon coated copper grid and was dried at room temperature. Fourier transform infrared (FT-IR) spectroscopic measurements were performed by a Thermo Nicolet Nexus 670 FT-IR spectroscope. The current−voltage ($I-V$) characteristics of CuTCNQ nanotube arrays were measured using a Keithley Semiconductor Characterization System (SCS-4200). Al electrodes are grounded, and voltage sweeps are applied on devices. All of the electrical measurements were made under ambient conditions.

**Fabrication of CuTCNQ Nanotube arrays.** A glass plate ($6 \times 4$ cm$^2$) spin coated with a TCNQ film (3 mg) was laid at the center of a quartz tube and a copper foil ($5.3 \times 4.6$ cm$^2$ with the thickness of 100 $\mu$m) was fixed on the top of glass plate. After the horizontal tube furnace was heated to 170 °C (for sample A), 150 °C (for sample B), and 190 °C (for sample C), respectively, the quartz tube loaded glass plate and copper foil was rapidly inserted in the tube furnace under argon gas flow (40 standard cubic centimeters per minute) and kept at that temperature for 15 min. A mass of TCNQ vapor was produced under instantaneous heating and reacted with copper on the top of glass plate to form CuTCNQ. Finally, the surface of the copper was deposited with a layer blue-green film, which indicated that the CuTCNQ nanotubes (samples A, B and C) grew successfully on the surface of copper.

## Results and Discussion

The as-preapred CuTCNQ nanotubes (sample A) are characterized by FT-IR spectra (Figure 1A), which provide evidence for bonding copper and TCNQ. CuTCNQ nanotubes show strong stretches at 2198 cm$^{-1}$. Compared with the spectrum of pure TCNQ molecule, the spectrum of CuTCNQ nanotubes shows obvious change. The absorption at 827 cm$^{-1}$ is consistent with the presence of $TCNQ^-$ and not TCNQ, $TCNQ^{2-}$, or mixed-valence stacks of $TCNQ^-$ and TCNQ,[5] which is very sensitive to change in oxidation state. The absorption of the CN group at 2198 cm$^{-1}$ indicates that the CuTCNQ nanotube is phase I of CuTCNQ.[6] The success of the preparing CuTCNQ nanotubes is further confirmed by XPS spectra (Figure 1B,C). The $2p_{3/2}$ and $2p_{1/2}$ signals (932.7 and 952.4 eV) exhibit essentially identical binding energies for Cu 2p orbital in accord with Cu(I).[7] Likewise, the $N_{1s}$ orbital appearing as a single feature at 399.66 eV is indicative of only one type of TCNQ.[8] The results indicate unambiguously that these nanotubes are composed of CuTCNQ.

Figure 2A displays the photographs of sample A prepared at 170 °C, whose areas are up to 24 cm$^2$. TEM images show that the CuTCNQ nanotubes are well-defined, straight, or gently curved with a smooth surface and with a total diameter between 150 to 300 nm, and an inner diameter of 10−50 nm (Figure 2B). Figure 2C shows a TEM image of a typical individual CuTCNQ nanotube with a 160 nm diameter and wall thickness of about 40 nm. The SAED pattern (Figure 2D) shows that the CuTCNQ nanotube is single crystal.[6] It suggests that the nanotubes grow along the [100] direction of the monoclinic CuTCNQ phase I structure, in which CuTCNQ molecules stacked up along this direction through strong $\pi-\pi$ interactions. The SEM images (Figure 2E) reveal that the blue-green film deposited on the surface of copper foil consists of vertically grown CuTCNQ nanotube arrays. Figure 2E is the cross-section SEM image of CuTCNQ nanotube arrays, which show the oriented nanotubes are vertically aligned. The lengths of CuTCNQ nanotubes are ranged from 5 to 20 $\mu$m. Interestingly, as shown in Figure 2F, the nanotubes are quadrate and the diameter is about 200 nm.

Decreasing the temperature of the reaction to 150 °C, as shown in Figure 3A, the CuTCNQ nanotube arrays (sample B) vertically grew on the copper foil. The lengths of CuTCNQ nanotubes are only several micrometers and the diameters are about 150 nm (the inset of Figure 3A). TEM image in Figure 3C demonstrates that the diameter and the thickness of wall of a typical CuTCNQ nanotube is 312 and 64 nm, respectively. The SAED pattern (the inset of Figure 3B) indicates that the CuTCNQ nanotube is a monoclinic CuTCNQ phase I structure. When the temperature of the

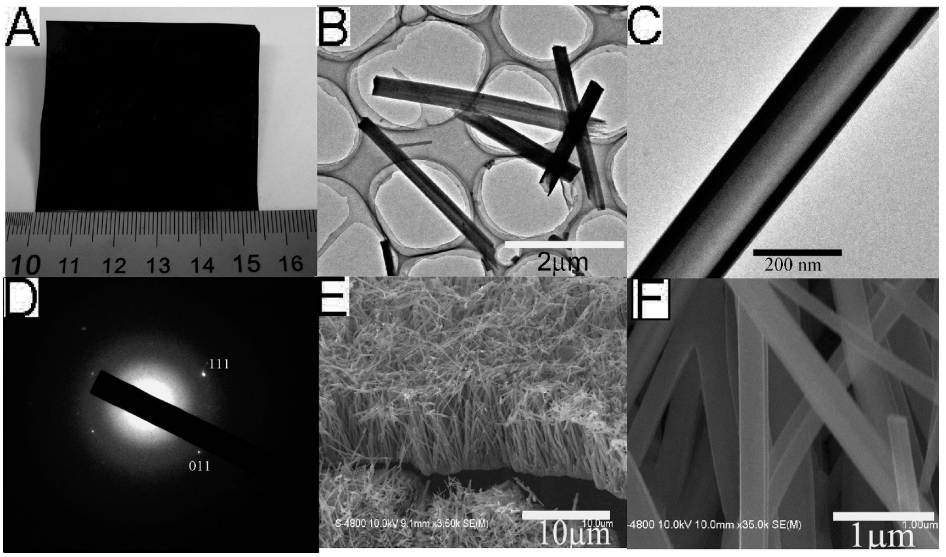


**Figure 2.** (A) Photograph of large-scale CuTCNQ nanotube arrays (sample A) on Cu foil. TEM image (sample A): (B) CuTCNQ nanotubes, (C) typical individual CuTCNQ nanotube, (D) the corresponding SAED pattern of CuTCNQ nanotube. SEM images of sample A: (E) cross-section and (F) higher magnifications.

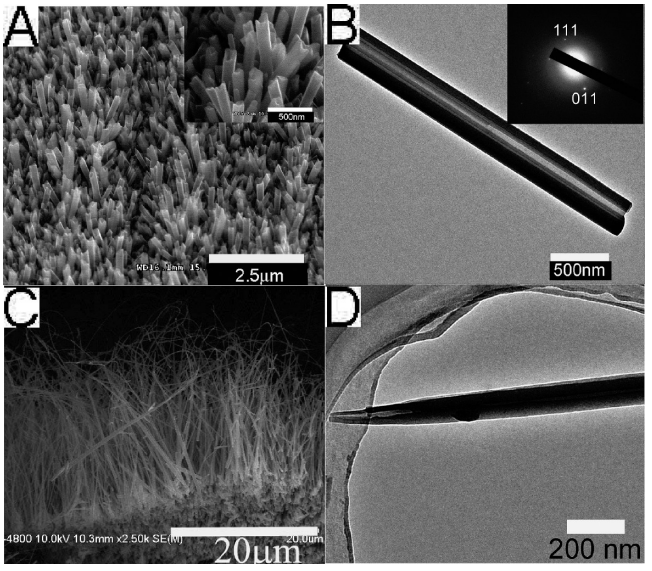


**Figure 3.** SEM image of sample B: (A) lower magnification and the inset is the corresponding higher magnification. (B) TEM image of a typical individual CuTCNQ nanotube; the inset is the corresponding SAED pattern of CuTCNQ nanotube. Sample C (D) cross-section of SEM image and (E) TEM image of a typical individual CuTCNQ nanotubes.

reaction is increased to 190 °C, the oriented CuTCNQ nanotubes (sample C) perpendicularly align on the copper foil and the lengths of nanotube increase to 12−50 $\mu$m (Figure 3D). The diameter of nanotube is smaller at the tip position than at the bottom position. As shown the TEM image in Figure 3E, the diameter of individual CuTCNQ nanotube on different positions exhibits diversity; the thickness of wall at the tip position is 30 and 10 nm, respectively, and at the middle position is 100 and 35 nm, respectively.

Figure 4 shows a schematic illustration of the growth of CuTCNQ nanotube arrays on Cu foil. The growing process is concomitant with a reaction of Cu and TCNQ molecules all the while. The growth mechanism of the CuTCNQ nanotube is similar to the growth of hollow and solid semiconductors.[9] The concentration of TCNQ vapor is the key effective factor to the growth and morphologies of the CuTCNQ complex, where the concentrations of TCNQ vapor can be controlled by adjusting the heating velocity. At first, a mass of TCNQ vapor is generated through instantaneous heating TCNQ film on a glass plate (Figure 4A), which leads to a high concentration of TCNQ vapor. The TCNQ vapor immediately reacts with metal copper on the surface of the Cu foil to form the CuTCNQ complex, which deposits to form nuclei that is seed particles (Figure 4B). At this high concentration of TCNQ vapor, the growth rate ($R_g$) is low with respect to the rate of diffusion ($R_f$) at the vapor−solid interface, and the copper concentrations are intensely decreased close to the top area of CuTCNQ nanostructures, inducing the preferential growth of nanotubes (Figure 4C,D) and limiting the growth of nanorods. This is a very interesting growing phenomenon that the diameter was decreased and the length of nanotubes was increased when increasing the growth temperature. In fact, the quantity of copper atoms from copper foil diffusing to the top of CuTCNQ nanotube gradually decreases due to extending the diffusion distance when increasing the length of the growing CuTCNQ nanotube. Therefore, the CuTCNQ nanotubes with uniform diameter are formed at 150 °C, and the diameter on the top of nanotube formed at 170 °C is slightly less than that on the bottom of the nanotube. When the temperature of instantaneous heating increases to 190 °C, the tip structure with hollow was formed on the top of nanotube. However, when the TCNQ film is gradually heated from room temperature (rt) to 170 °C, a low concentration of TCNQ vapor is produced during the process of gradually heating due to the TCNQ vapor that can be generated from TCNQ film at 80 °C. At low concentrations of TCNQ vapor, the crystal growth is relatively fast with respect to the diffusion rate at the vapor−solid interface. Growth takes place at the entire vapor−solid interface, giving rise to solid nanowires (Figure 4E). As shown in Figure 5, the CuTCNQ nanowires with a diameter of 100 nm are obtained when the copper foil fixed on the top of the glass plate coated TCNQ film is gradually heated from room temperature to 170 °C. The results confirm this proposed growth mechanism.

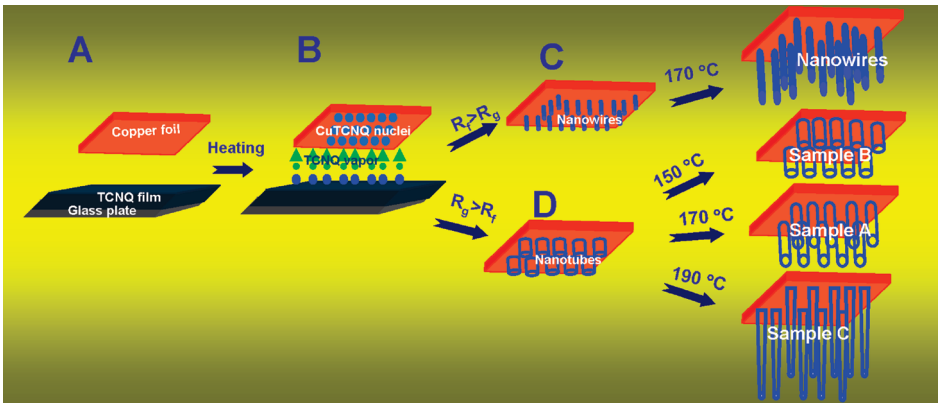


**Figure 4.** Schematic illustration of the growth of CuTCNQ nanotube arrays on Cu foil.

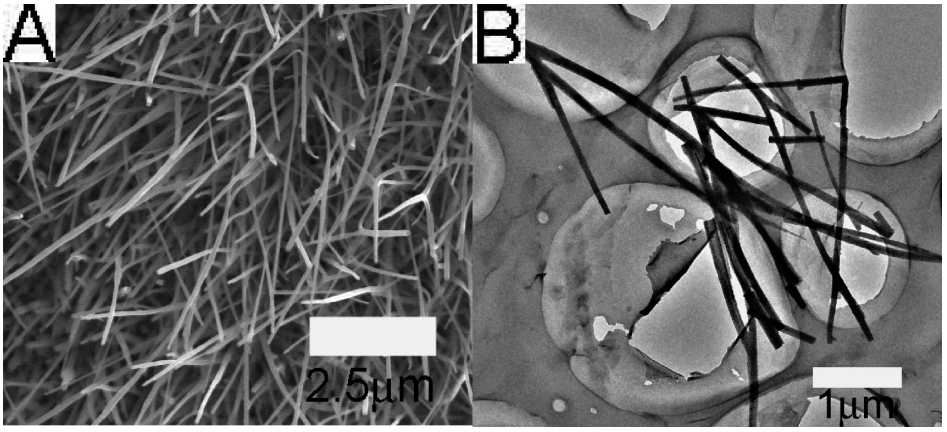


**Figure 5.** (A) SEM image of CuTCNQ nanowires. (B) TEM image of CuTCNQ nanowires.

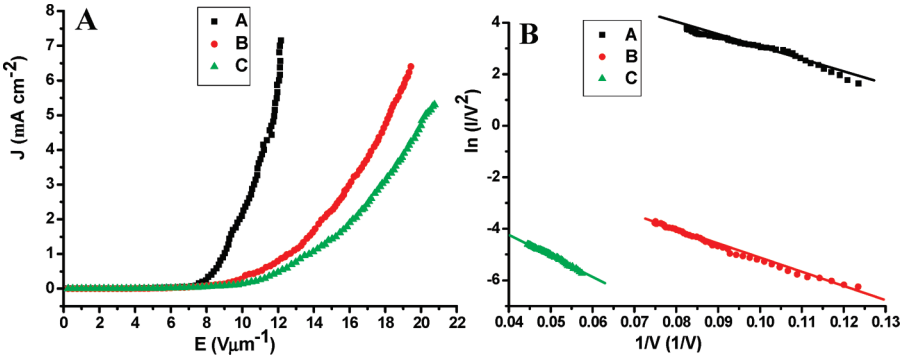


**Figure 6.** (A) Field emission $J-E$ curve of the CuTCNQ nanotube arrays and (B) the corresponding FN plot.

**Field Emission Properties.** As expected from the CuTCNQ nanotube arrays, their excellent FE properties were observed. We performed the FE measurements on the arrays of organic charge transfer complex CuTCNQ nanotube with different sizes. Figure 6A shows a typical plot of the FE current density versus the applied electric field ($J-E$ plot) of the CuTCNQ nanotubes prepared under different temperatures on the surface of copper foil. The turn-on field ($E_{to}$) and threshold field ($E_{thr}$) are defined as the macroscopic field required to produce a current density of 10 $\mu$A/cm$^2$ and 1 mA/cm$^2$, respectively. As shown in Figure 6A, the $E_{to}$ of sample A, B, and C is 4.49, 5.25, and 4.99 V/$\mu$m, respectively. They are higher than that of CuTCNQ nanowires, but the maximal current density for sample A is 7.15 mA/cm$^2$ under the applied field about 12.2 V/$\mu$m. The result is 11.6 times more than that of CuTCNQ nanowires.[4f] The maximal current density for samples B and C is 5.3 and 6.4 mA/cm$^2$, under the applied field of about 20.8 and 19.4 V/$\mu$m, respectively. This is because the emitter radius of CuTCNQ nanotubes is smaller than that of CuTCNQ nanowires. The field emission characteristics were analyzed using the Fowler−Nordheim (F−N) model described as follows:[10]

$$J = (A\beta^2E^2/\Phi)\exp(-B\Phi^{3/2}/\beta E) \quad (1)$$

where $A = 1.54 \times 10{-}6$ A eV V$^{-2}$, $B = 6.83 \times 103$ eV$^{-3/2}$ $\mu$m$^{-1}$, $\Phi$ is the work function of the emitter, and $\beta$ is the field enhancement factor. The insets of Figure 6B, the variation of $\ln(J/E^2)$ with $(1/E)$ is a rough straight line, indicate that FE

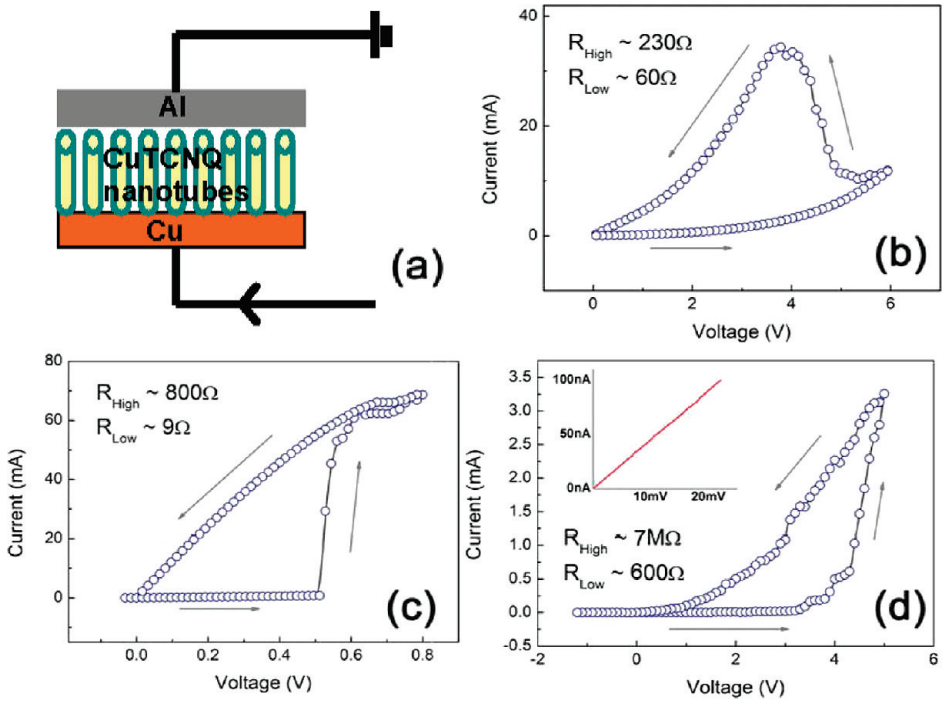


**Figure 7.** (a) Illustration of the circuit of device under testing. Cu foil and Al film are taken as the bottom electrode and top electrode, respectively. Samples are grown on Cu films and the area of Al films is about 20 $mm^2$. Voltage sweeping applied to various structures of CuTCNQ. Panels (b−d) show typical $I-V$ curves for three different samples. Arrows indicate the direction of voltage sweeping. Inset in (d) indicates a high resistance state under low current sweeping (0−100 nA).

processes from the CuTCNQ nanotube arrays are a quantum tunneling process. Assuming $\Phi = 2.77$ eV for CuTCNQ,[4f] the field enhancement factors $\beta$ are 699, 374, and 508 for the CuTCNQ nanotube arrays A, B, and C, respectively. The value of $\beta$ relates to the structure, shape, size, alignment, crystallinity, aspect ratio, etc.[11] It is generally accepted that the enhancement factor $\beta$ is not only determined by the aspect ratio but also by the ratio of length to the wall thickness for the tube-like emitters.[12] For those samples with the same structure, shape, and crysallinity, they are different from the aspect ratio and the ratio of length to wall thickness. From Figure 3, the aspect ratio of sample B and the ratio of length to wall thickness are lower than that of sample A. Although the aspect ratios and the ratio of length to wall thickness of sample C are more than that of sample A, the alignments of sample C are lower than that of sample A because their lengths are too long to be entangled with each other in nanotube arrays, which lead to a decrease in the value of $\beta$. Therefore, the field emission property of sample A is better than that of samples B and C.

**Electrical-Switching.** The devices based on those CuTCNQ nanotube arrays and nanowires were fabricated on the Cu foils. Three different nanostructures of CuTCNQ samples (nanowires, A and B) are grown on Cu foils as bottom electrodes, and Al films are prepared as top electrodes (about 20 $mm^2$),[13,14] illustrated by Figure 7. We observed evolution in conducting transition for different samples. For CuTCNQ nanowires, the typical $I-V$ curve in Figure 7b exhibits a switching effect at high voltage, with an ON/OFF ratio ~ 10 at 4 V. Figure 7c shows the $I-V$ characterization for CuTCNQ short nanotubes (sample B); the voltage threshold ranges from 500 to 800 mV, far less than the value of CuTCNQ nanowires. Furthermore, an ON/OFF ratio ~ 70 is obtained. It is indicated that, compared to nanowires, nanotubes possess higher performances on the electrical switching effect, which is confirmed by following measurements on long nanotubes of CuTCNQ (sample A). As shown in Figure 7d, long CuTCNQ nanotubes exhibit excellent switching performance on ON/OFF ratio which is about 1100 at less than 1.25 V. However, when the applied voltage is less than 1.2 V, the current remains about 200 nA, whose slope shows great conduction far more than 1000.

There are several important points that should be emphasized. First of all, we observed two switching transitions: high voltage switching effect (HVSE) and low voltage switching effect (LVSE). HVSE can be observed for all samples and LVSE for only nanotubes; the phase transition may responsible for these two states. Second, it can be seen that, for HVSE both the "ON" and "OFF" conduction states are almost exponential, compared to the linear (Ohmic) for the LVSE case. It is indicated that the resistance relies on the electric field strength for HVSE and is independent for LVSE. Furthermore, asymmetrical $I-V$ curves are observed for all samples, demonstrating electrodes dependence properties for the conducting of CuTCNQ. It is well-known that the phase transition plays an important role in the switching effect. Before phase transition in CuTCNQ, the overlap of $\pi$ orbitals dominates their conducting. And $Cu^0$ would contribute to the increase of conducting after the phase transition.[6] Compared to nanowires, CuTCNQ nanotubes are more stable for their relative low density. Meanwhile, the tube structure of CuTCNQ is an advantage for the transport of carrier supplied by metallic $Cu^0$. As a result, nanotubes exhibit a better performance on electrical switching effect and LVSE can be realized.

The low ON/OFF ratio of CuTCNQ nanowires is shown in Figure 8a. Their large length−diameter ratio (20−40) results in a flexible state, and therefore leading to a network-like

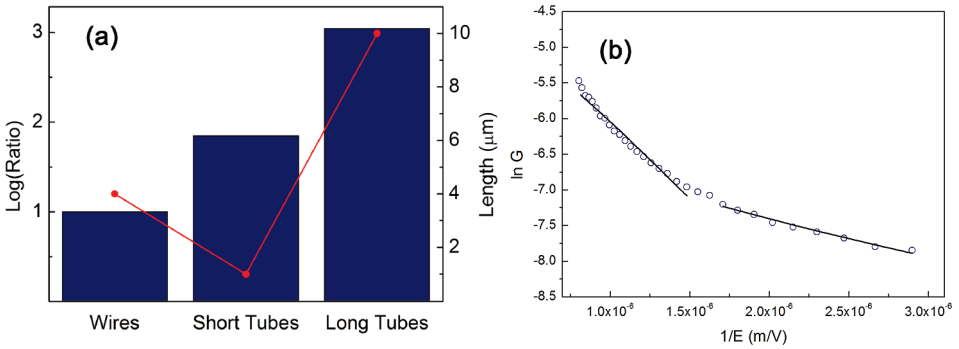


**Figure 8.** (a) Illustration of the electric switch ratio for CuTCNQ nanowires and nanotubes (navy bar) with red dots indicating the length sample. The performance of electric switch effect showed an exponential increase from nanowires, short nanotubes (sample B) to long nanotubes (sample A), depending on the morphology. (b) The electric field dependence of conduction for CuTCNQ nanowires. The black line is three parameters data fitting for ln $G \sim 1/E$ curve.

contact with Al electrodes. Electric-field dependence is described by an equation:[15]

$$G(E) = G_0 \exp[-(E_0/E)^{\Delta}] \quad (2)$$

This equation can be rewritten as

$$\ln G = -(E_0/E)^{\Delta} + \ln G_0 \quad (3)$$

According to Figure 8b, transition of ln $G$ versus $1/E$ can be observed. By data fitting (solid line), G0 and $\Delta$ are 0.6 and 4 mS at the low voltage region, and 1.2 and 10 mS at the high voltage region, respectively. $E_0$ is about 15000 V/cm for both regions. We attribute this transition to the confined heat effect, which would damage samples or increase the phase transition rate from CuTCNQ to $[Cu^0]_x$, $[TCNQ^0]_x$, $[Cu^+(TCNQ^-)]_{n-x}$.[3] It has been confirmed by repeated measurements for a sample. So it is difficult for us to observe the large ON/OFF ratio for nanowires. However, for CuTCNQ nanotubes, their unique structure ensures their safety from heat, and only a few tubes are contacting Al electrodes, and overlaps of $\pi$ orbitals supply an increasing transport channel for $Cu^0$ carriers. For long nanotubes, an electric switch effect is beneficial for efficient heat dissipation and few nanotubes contacting the electrodes. It also demonstrates clearly that long nanotubes have better performance than short ones.

## Conclusions

In summary, large-scale single crystalline CuTCNQ nanotube arrays have been synthesized using an in situ organic vapor solid phase reaction by instantaneous heating. This facile approach provides an important finding for large area synthesis of vertically aligned array organic nanotubes on conductive substrate. The size of CuTCNQ nanotubes can be tuned by controlling the reaction temperature. This selective growth of CuTCNQ nanotube arrays on conductive substrate is crucial to the direct fabricating of electronic and optoelectronic devices for a wide variety of potential applications. The CuTCNQ nanotube arrays exhibited excellent FE properties and size-dependent FE properties were observed. The maximal current density for CuTCNQ nanotube arrays is 7.15 mA/cm$^2$, which is 11.6 times more than that of CuTCNQ nanowires. The devices based on those nanotubes and nanowires have been built and switched electrically between two states with a conductivity difference. The morphology-dependent electric-switching properties of the CuTCNQ nanotube arrays are observed. Long CuTCNQ nanotube arrays show a high ON/OFF ratio $\sim$ 1100. The nanotube array is an excellent candidate for further studies in organic electronics.

**Acknowledgment.** This work was supported by the National Nature Science Foundation of China (20531060, 20721061, and 20571078) and the National Basic Research 973 Program of China.

## References

(1) (a) Yamamoto, Y.; Fukushima, T.; Suna, Y.; Ishii, N.; Saeki, A.; Seki, S.; Tagawa, S.; Taniguchi, M.; Aida, T. *Science* **2006**, *314*, 1761–1763. (b) Hoeben, F. J. M.; Jonkheijm, P.; Meijer, E. W.; Schenning, A. P. H. *J. Chem. Rev.* **2005**, *105*, 1491–1512. (c) Grimsdale, A. C.; Mullen, K. *Angew. Chem., Int. Ed.* **2005**, *44*, 5592–5595. (d) Nguyen, T. Q.; Martel, R.; Avouris, P.; Bushey, M. L.; Brus, L.; Nuckolls, C. *J. Am. Chem. Soc.* **2004**, *126*, 5234–5235. (e) Zhang, X. J.; Zhang, X. H.; Shi, W. S.; Meng, X. M.; Lee, C. S.; Lee, S. T. *Angew. Chem., Int. Ed.* **2007**, *46*, 1525–1528. (f) Lu, K.; Jacob, J.; Thiyagarajan, P.; Conticello, V. P.; Lynn, D. G. *J. Am. Chem. Soc.* **2003**, *125*, 6391–6392. (g) Sun, Y. H.; Ye, K. Q.; Zhang, H. Y.; Zhang, J. H.; Zhao, L.; Li, B.; Yang, G. D.; Yang, B.; Wang, Y.; Lai, S. W.; Che, C. M. *Angew. Chem., Int. Ed.* **2006**, *45*, 5610–5613.

(2) (a) Modi, A.; Koratkar, N.; Lass, E.; Wei, B. Q; Ajayan, P. M. *Nature* **2003**, *424*, 171–174. (b) Karp, E. S.; Inbaraj, J. J.; Laryukhin, M. *J. Am. Chem. Soc.* **2006**, *128*, 12070–12071. (c) Guo, J.; Farmer, D. B.; Wang, Q.; Yenilmez, E.; Gordon, R. G.; Lundstrom, M.; Dai, H. J. *Nano Lett.* **2004**, *4*, 1319–1322.

(3) (a) Bong, D. T.; Clark, T. D.; Granja, J. R.; Ghadiri, M. R. *Angew. Chem., Int. Ed.* **2001**, *40*, 988–1011. (b) Zhang, X. J.; Ju, W. G.; Gu, M. M.; Zhang, X. H.; Meng, X. M.; Shi, W. S.; Lee, C. S.; Lee, S. T. *Chem. Commun.* **2005**, *33*, 4202–4203. (c) Liu, H. B.; Li, Y. L.; Jiang, L.; Luo, H. Y.; Xiao, S. Q.; Fang, H. J.; Li, H. M.; Zhu, D. B.; Yu, D. P.; Xu, J.; Xiang, B. *J. Am. Chem. Soc.* **2002**, *124*, 13370–13371. (d) Steinhart, M.; Wendorff, J. H.; Greiner, A.; Wehrspohn, R. B.; Nielsch, K.; Choi, J.; Gosele, U. *Science* **2002**, *296*, 1997–1997.

(4) (a) Muller, R.; Genoe, J.; Heremans, P. *Appl. Phys. Lett.* **2006**, 88–90. (b) Muller, R.; De Jonge, S.; Myny, K.; Wouters, D. J.; Genoe, J.; Heremans, P. *Solid-State Electron.* **2006**, *50*, 602. (c) Zhong, C.; Jiang, Y.; Luo, Y.; Liao, J.; Wu, W.; Li, J. *Acta Phys.-Chim. Sin.* **2006**, *22*, 696. (d) O'Mullane, A. P.; Neufeld, A. K.; Bond, A. M. *Anal. Chem.* **2005**, *77*, 5447–5451. (e) Neufeld, A. K.; O'Mullane, A. P.; Bond, A. M. *J. Am. Chem. Soc.* **2005**, *127*, 13846–13851. (f) Liu, H. B.; Zhao, Q.; Li, Y. L.; Liu, Y.; Lu, F. S.; Zhuang, J. P.; Wang, S.; Jiang, L.; Zhu, D. B.; Yu, D. P.; Chi, L. F. *J. Am. Chem. Soc.* **2005**, *127*, 1120–1121. (g) O'Mullane, A. P.; Fay, N.; Nafady, A.; Bond, A. M. *J. Am. Chem. Soc.* **2007**, *129*, 2066–2073. (h) Sun, W. L.; Li, Y. X.; Liu, H. B.; Li, YY. L.; Gan, H. Y.; Jiu, T. G.; Li, Y. J.; He, X. R.; Wang, N.; Jiang, L. *Chem. J. Int.* **2006**, *8*, 080639ne. (i) Tian, F.; Liu, W.; Wang, C. R. *J. Phys. Chem. C* **2008**, *112*, 8763–8766. (j) Harris, A. R.; Neufeld, A. K.; O'Mullane, A. P.; Bond, A. M.; Morrison, R. J. S. *J. Electrochem. Soc.* **2005**, *152*, C577. (k) Fan, Z. Y.; Mo, X. L.; Lou, C. F.; Yao, Y.; Wang, D. W.; Chen, G. R.; Lu, J. G. *IEEE Trans. Nanotech* **2005**, *4*, 238–244. (l) Cao, G.; Ye, C.; Fang, F.; Xing, X.; Xu, H.; Sun, D.; Chen, G. *Mater. Sci. Eng., B* **2005**, *119*, 41–45. (m) Liu, Y. L.; Ji, Z. Y.; Tang, Q. X.; Jiang, L.; Li, H. X.; He, M.; Hu, W. P.; Zhang, D. Q.; Wang, X. K.;

Wang, C.; Liu, Y. Q.; Zhu, D. B. *Adv. Mater.* **2005**, *17*, 2953–2958. (n) Oyamada, T.; Tanaka, H.; Matsushige, K.; Sasabe, H.; Adachi, C. *Appl. Phys. Lett.* **2003**, *83*, 1252–1255. (o) Neufeld, A. K.; Madsen, I.; Bond, A. M.; Hogan, C. F. *Chem. Mater.* **2003**, *15*, 3573–3578. (p) Liu, H. B.; Wu, X. C.; Chi, L. F.; Zhong, D. Y.; Zhao, Q.; Li, Y. L.; Yu, D. P.; Fuchs, H.; Zhu, D. B. *J. Phys. Chem. C* **2008**, *112*, 17625–1730. (q) Liu, H. B.; Cui, S.; Guo, Y. B.; Li, Y. L.; Huang, C. S.; Zuo, Z. C.; Yin, X. D.; Song, Y. L.; Zhu, D. B. *J. Mater. Chem.* **2009**, *19*, 1031–1036.

(5) (a) Kobayashi, A.; Kato, R.; Kobayashi, H.; Mori, T.; Inokuchi, H. *Solid State Commun.* **1987**, *64*, 45. (b) Yashihiro, Y.; Furukawa, Y.; Kobayashi, A.; Tasumi, M.; Kato, R.; Kobayashi, H. *J. Chem. Phys.* **1994**, *100*, 2449–2453.

(6) Heintz, R. A.; Zhao, H.; Ouyang, X.; Grandinetti, G.; Cowen, J.; Dunbar, K. R. *Inorg. Chem.* **1999**, *38*, 144–156.

(7) (a) Potember, R. S.; Poehler, T. O.; Cowan, D. O.; Carter, F. L.; Brant, P. I. *In Molecular Electronic Devices*; Carter, F. L., Ed.; Marcel Dekker: New York, 1982; p 73; (b) Potember, R. S.; Poehler, T. O.; Cowan, D. O.; Brant, P.; Carter, F. L; Bloch, A. N. *Chem. Scr.* **1981**, *17*, 219–223.

(8) Ikemoto, I.; Thomas, J. M.; Kuroda, H. *Bull. Chem. Soc. Jpn.* **1973**, *46*, 2237–2241.

(9) Bakkers, E. P. A. M.; Verheijen, M. A. *J. Am. Chem. Soc.* **2003**, *125*, 3440–3441.

(10) Fowler, R. H.; Nordheim, L. W. *Proc. R. Soc. London, Ser. A* **1928**, *119*, 173–177.

(11) Lee, C. J.; Lee, T. J.; Lyu, S. C.; Zhang, Y.; Ruh, H.; Lee, H. J. *Appl. Phys. Lett.* **2002**, *81*, 3648–3650.

(12) (a) Kokkorakis, G. C.; Modinos, A.; Xanthakis, J. P. *J. Appl. Phys.* **2002**, *91*, 4580–4587. (b) Kokkorakis, G. C.; Roumeliotis, J. A.; Xanthakis, J. P. *J. Appl. Phys.* **2004**, *95*, 1468–1471.

(13) Muller, R.; Naulaerts, R.; Billen, J.; Genoe, J.; Heremans, P. *Appl. Phys. Lett.* **2007**, *90*, 063503.

(14) Kever, T.; Bottger, U.; Schindler, C.; Waser, R. *Appl. Phys. Lett.* **2007**, *91*, 083506.

(15) (a) Liu, G.; Soonpaa, H. H. *Phys. Rev. B* **1993**, *48*, 5682–5688. (b) Licciardello, D. C.; Soonpaa, H. H. *Surf. Sci.* **1980**, *98*, 225–226. (c) Jana, D.; Fort, J. *Physica B: Condensed Matter* **2004**, *344*, 62–65.